SIMULATIONS OF OPTICAL TURBULENCE VIA NUMERICAL WEATHER PREDICTION FOR USE IN OPTICAL COMMUNICATION STUDIES

Randall J. Alliss, Billy D. Felton, and Eric M. Kemp

Northrop Grumman Information Technology/TASC
4801 Stonecroft Blvd.
Chantilly, VA 20151

Abstract

Optical turbulence (OT) acts to distort light in the atmosphere, degrading imagery from large astronomical telescopes and possibly reducing data quality of laser communication links. Some of the degradation due to turbulence can be corrected by adaptive optics. However, the severity of OT, and thus the amount of correction required, is largely dependent on the turbulence at the location of interest. Therefore, it is vital to understand the climatology of OT at such locations. In many cases, it is impractical and expensive to set up instrumentation to characterize the climatology of OT, so simulations become a less expensive and convenient alternative.

The strength of OT is characterized by the refractive index structure function C_n^2, which in turn is used to calculate atmospheric seeing parameters. Although attempts have been made to characterize C_n^2 using empirical models, C_n^2 can be calculated more directly from Numerical Weather Prediction (NWP) simulations using pressure, temperature, thermal stability, vertical wind shear, turbulent Prandtl number, and turbulence kinetic energy (TKE). In this work we use the Weather Research and Forecasting (WRF) NWP model to generate C_n^2 climatologies in the planetary boundary layer and free atmosphere, allowing both point-to-point and ground-to-space seeing estimates of the Fried Coherence length (r_o) and other seeing parameters. Simulations are performed using the Maui High Performance Computing Center's Jaws cluster.

The WRF model is configured to run at 1-km horizontal resolution over a ~60-km by 60-km domain. The vertical resolution varies from 25 m in the boundary layer to 500 m in the stratosphere. The model top is 20 km. The Mellor-Yamada-Janjic (MYJ) TKE scheme has been modified to diagnose the turbulent Prandtl number as a function of the Richardson number, following observations by Kondo and others. This modification deweights the contribution of the buoyancy term in the equation for TKE by reducing the ratio of the eddy diffusivity of heat to momentum. This is necessary particularly in the stably stratified free atmosphere where turbulence occurs in thin layers not typically resolvable by the model. The modified MYJ scheme increases the probability and strength of TKE in thermally stable conditions, thereby increasing the probability of OT. Over 12 months of simulations have been generated. Results indicate realistic values of the r_o are obtained when compared with observations from a Differential Image Motion Monitor instrument. Seeing is worse during day than at night with large r_o's observed just after sunset and just before sunrise. Three-dimensional maps indicate how seeing varies as a function of location and elevation. This study has shown that urban heat islands and nighttime low-level jets can greatly influence the production of OT. Detailed results of this study will be presented at the conference.

1. Introduction

With High Performance Computing (HPC) platforms becoming much more affordable and accessible, simulations of physical quantities in the atmosphere are easily performed. An excellent example of this is free space optical turbulence (OT). OT is an important atmospheric phenomenon, particularly for astronomers, because of the impact it has on seeing. Small-scale temperature and moisture fluctuations in the atmosphere result in fluctuations of the refractive index. The wave front of radiation traveling through the atmosphere changes as it encounters inhomogeneities in the refractive index, degrading optical image quality. The intensity of the turbulent fluctuations of the atmospheric refractive index is described by the refractive index structure function, C_n^2. The ability to quantify the amount of OT above an observatory and to understand its vertical distribution is vital and can impact decisions on adaptive optics design, observatory scheduling, and site selection for new observatories. Although instruments have been developed to characterize OT, they are expensive to maintain over long durations of time and the quality is limited.

Numerical simulations of OT are an attractive alternative to local observations in regions where infrastructure (i.e., electrical power) is lacking. Numerical simulations offer many advantages over direct measurements. These advantages include a three-dimensional description of C_n^2 over regions of interest, simulations that can be performed anywhere on earth at any time, and the ability to provide forecasts of OT that could be used for

observational scheduling purposes. The reliability of these types of simulations for describing the climatology of OT has recently been shown to be quite good.

Our approach to simulate OT employs a model used to predict tropospheric weather. These models are referred to by the meteorological community as Numerical Weather Prediction (NWP). NWP models are routinely used by meteorologists to predict everyday weather. However, in this application the model is modified to make simulations of C_n^2. In this paper we describe how NWP is leveraged to simulate OT and present various results along with intercomparisons to direct observations of integrated OT.

2. Technical Approach

In this study we use version 2.2 of the Weather Research and Forecasting (WRF) model developed jointly by the National Center for Atmospheric Research (NCAR) and the National Oceanic and Atmospheric Administration (NOAA) (Skamarock et al., 2008). WRF is a mesoscale NWP model developed for the prediction of weather and is routinely used by the National Weather Service and other forecasting services. The model is based on the Navier Stokes equations, which are solved numerically on a three-dimensional grid. Four basic atmospheric properties are simulated by the model from which all others variables are derived. These properties are wind, pressure, temperature, and atmospheric water vapor.

This study used the WRF model to develop climatologies of OT for several regions over the continental United States. The following sections describe the model setup, modifications to the code, and derivation of OT parameters followed by results of simulations to date.

a. Model Setup

WRF is used to simulate daily meteorological conditions for several regions in the United States for the period 2006–2007. In each case the model is configured at 1-km horizontal resolution with dimensions 67×63. The number of vertical grid points varies from 135 to 140, with the sigma levels set to approximate 50-m resolution below 2 km above ground level (AGL), 125 m for 2–12 km AGL, and 500 m up to the model top (50 millibars). Simulations are initialized at 1200 UTC directly from the 12-km North American Mesoscale (NAM) analysis produced by the National Weather Service. Lateral boundary conditions are provided out to 27 hours by three-hourly NAM forecasts. This allows for filtering out model "spin-up" by excluding the first three simulation hours, while still capturing the full 24-hour diurnal cycle. Selected physics and diffusion options are summarized in Table 1.

Table 1. Physics and diffusion settings used in WRF model for this study

Time Integration	RK3
Time Step	2 sec
Horizontal/Vertical Advection	Fifth/Third order
Explicit Diffusion	Physical space 2D deformation, no sixth order
Boundary Layer Physics	Mellor, Yamada, Janjic (MYJ)
Surface Layer	Janjic Eta
Land Surface	Noah
Shortwave/Longwave Radiation	Dudhia/RRTM
Microphysics	WSM6
Cumulus Parameterization	None

In general, the model was run once per day for approximately a 15-month period spanning 2006–2007.

b. Model Modifications

The minimum turbulence kinetic energy (TKE) permitted in the Mellor-Yamada-Janjic (MYJ) scheme had to be modified. The default setting gives TKE values >0.1 m^2s^{-2}, resulting in unrealistically large values of C_n^2 in the free atmosphere. Following Gerrity et al. (1994), the minimum TKE limit was changed to 10^{-5} m^2s^{-2}. The second modification involves the eddy diffusivities of heat and momentum (K_H and K_M, respectively). In the original MYJ scheme, these variables are given by

$$K_h = l_q S_H \quad , K_h = l_q S_M,$$

Where l is the mixing length, $q = \sqrt{2TKE}$, and S_H, and S_M, are functions of TKE, mixing length, buoyancy, and vertical wind shear (Mellor and Yamada, 1982). In the modified version these relationships are unchanged for neutral and unstable conditions. However, when the gradient Richardson number (Ri) > 0.01, an implementation by Walters and Miller (1999) is followed whereby K_M is adjusted according to:

$$\frac{K_H}{K_M} = \begin{cases} \dfrac{1}{7Ri}, & for Ri \geq 1, \\[2em] \dfrac{1}{6.873Ri + \dfrac{1}{1+6.873Ri}} & for 0.01 < Ri \leq 1. \end{cases}$$

The $\dfrac{K_H}{K_M}$ equation was first proposed by Kondo et al. (1978). The Kondo equation decreases $\dfrac{K_H}{K_M}$ with increasing Ri, effectively increasing the TKE production by vertical wind shear. This is necessary to generate free atmospheric turbulence that is commonly associated with jet streams. Without this change the model rarely produces TKE larger than the model's minimum value, something that is considered unrealistic when compared to many global thermosonde measurements (Ruggiero, personal communication, 2008).

c. Derivation of Seeing

This study is interested in the vertical distribution of the refractive index structure function C_n^2. When turbulence is locally homogeneous and isotropic, C_n^2 is related to changes in the refractive index. Large values of C_n^2 correspond to increasing changes in the refractive index and thus greater turbulence. Tatarskii (1971) derived an alternative expression for the structure function parameter applicable for optical wavelengths:

$$C_n^2 = \left(\frac{79 * 10^{-8} P}{T^2} \right)^2 C_T^2$$

where P is atmospheric pressure, T is air temperature, and C_T^2 is the structure function parameter for temperature. C_T^2 is given by:

$$C_T^2 = a^2 \left(\frac{K_H}{K_M} \right) L_o^{\frac{4}{3}} \left(\frac{\partial \theta}{\partial Z} \right)^2$$

Where a^2 is an empirical constant, L_o is the outer length scale of turbulence (i.e., the upper bound of the inertial subrange), and $\left(\dfrac{\partial \theta}{\partial Z} \right)$ is the vertical gradient of potential temperature. Following Walters and Miller (1999), a^2 is set to 2.8 and calculation of the outer length scale of turbulence in the thermally stable conditions is approximated from Deardorff (1980):

$$L_o = 0.76 \sqrt{\frac{TKE}{N}}$$

where N is the Brunt-Vaisala frequency. In thermally unstable conditions, L_o is related to the depth of the unstable boundary layer.

In this study we also compute Fried's Coherence Length (r_o), which is a measure of phase distortion of an optical wave front by turbulence. After Fried (1965), it is calculated by integrating C_n^2 along a path, z:

$$r_o = \left[0.423 \left(\frac{2\Pi}{\lambda} \right)^2 \int_0^\infty C_n^2(z)dz \right]^{-3/5}$$

3. Results

Three-dimensional turbulence simulations were made over the state of New Mexico once per day during 2007. These simulations took over 1200 wall clock hours on a 256 core Itanium cluster located at Northrop Grumman IT Headquarters. More recent simulations are being performed on the 5000 core Jaws Xeon cluster located at the Maui High Performance Computing Center (MHPCC).

Because the model output contains many terabytes of information a tool was developed to facilitate analysis of these data. Figure 1 shows a screen shot of the WRF Turbulence Viewer. This tool makes use of the Python scripting language to control data ingest and graphical user interface attributes and Matlab for data display. The tool provides a two-dimensional view of the topography over the selected domain. In this example the domain is centered on Albuquerque, NM (ABQ). Note the North-South oriented Sandia and Manzano Mountains located immediately to the east of ABQ. The tool allows the user to load any month or year of data and to quickly look at tw0-dimensional plots of various seeing parameters including r_o, Θ_o and the Greenwood Frequency, f_G, as a function of time of day. This allows for analysis of how the turbulence may be distributed horizontally across

Figure 1. Example of the WRF Turbulence Viewer

the domain. The user may also look at the distribution of any of these parameters for a single vertical column in the domain. In addition, the tool allows the overlay of turbulence data collected from a Differential Image Motion Monitor (DIMM) instrument for comparison purposes. In this case r_o data collected at the Starfire Optical Range (SOR) are used to compare against all WRF simulations.
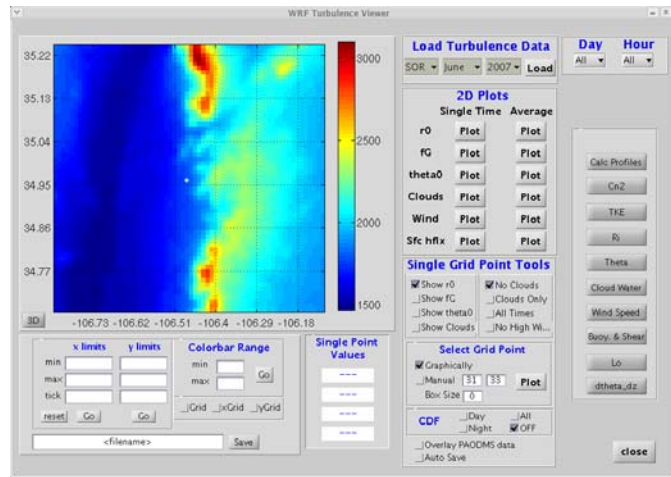
Figure 2 summarizes a year of simulations over ABQ in a time/height plot of C_n^2 (i.e., Hovmoller diagram). Data are plotted every hour during the year for each of the 137 vertical levels. The data show how C_n^2 varies with time. Red shaded ($\sim 10^{-14}$) areas denote higher turbulence, and darker blue shades ($\sim 10^{-18}$) indicate where turbulence is more benign. The figure indicates that the highest values of C_n^2 are found in the boundary layer (lowest 1.5 km). This is to be expected because solar insolation at the ground produces large heat fluxes, resulting in greater turbulence. Values can be as high as 10^{-13} on a hot summer afternoon when solar heating of the desert produces very large heat fluxes. Although the diurnal variation in C_n^2 is not visible in this figure, a large variation does exist (see later figures). Above the boundary layer, the C_n^2 profile becomes smaller until the jet stream level is reached. The height of jet can vary between 8 and 12 km depending on the time of year. Generally C_n^2 is larger during the winter months at these altitudes and smaller during the summer months as the jet weakens and retreats poleward. Typical values simulated during winter are 10^{-16} and 10^{-17} during the summer months.
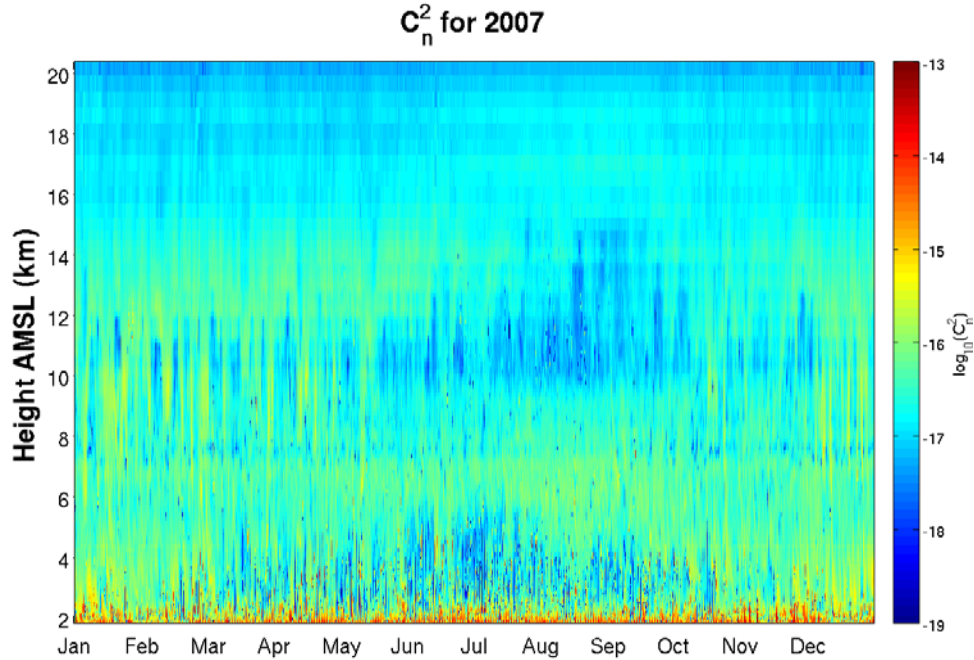
Figure 2. Cn^2 as a function of time and height over Albuquerque, NM, during 2007

The r_o was derived from the C_n^2 profiles in order to study its variation seasonally and diurnally. For comparison purposes we show how the climatology of r_o compares with measurements from a DIMM instrument located at the SOR. Figure 3 shows the diurnal variation of r_o for spring, summer, fall, and winter. The error bars at each hour indicate the 5th and 95th percentile of the observations (red) and simulations (blue), respectively. All data are referenced to zenith. The figure shows a remarkable similarity between observations and WRF simulations. The diurnal variation is clearly evident with r_o dropping during the daylight hours and rising near sunset. The observations indicate an increase in r_o just after sunrise and just before sunset. This occurs when the lower atmosphere becomes decoupled from the free atmosphere and the temperature lapse rate shows a neutral stability thereby suppressing turbulence. This daily event, known as the neutral event, has long been observed in OT measurements and is also simulated nicely by WRF. The diurnal variation is most noticeable in the spring and summer months and less so during the cool seasons. Day/night differences in r_o range from 5 cm during the warm months to approximately 2 cm during the cool season when the surface heat flux is reduced due to low sun angles and more cloud cover. The overlap in the distributions between the simulations and observations is also quite remarkable. However, in general, the WRF model does not simulate the lowest r_o. This is not surprising given the differences in resolution between the model and the DIMM instrument. WRF is run with a horizontal resolution of one kilometer whereas the instrument is taking measurements in the line of sight of a star. Therefore, it is expected the WRF model will only see the mean turbulence over that 1-km area. The 95th percentile r_o values from the instrument are estimated to be around 1.5 cm during the daytime while simulations from WRF are approximately 2 cm.

Although WRF is unable to simulate the lowest r_o during the daytime, it is simulating lower r_o than observations at night. This is particularly true during the spring and fall months. Upon further investigation, the WRF model is doing an excellent job in simulating the canyon winds that are typical at night in this area. They are most pronounced during the spring and fall months under clear skies with high pressure centered to the northeast of ABQ. This condition sets up an easterly wind that is accelerated through the Sandia and Manzano passages underneath a strong temperature inversion. Winds during these events can easily exceed 20 ms^{-1}. The result is typically more turbulence. When winds exceeded 10 ms^{-1}, the dome in which the DIMM was located was closed, thereby eliminating any observations during those times. Therefore, we believe the observational climatology of r_o at this location may be affected at nighttime due to lack of observations. Indeed, there are many fewer observations between 0600 and 1200 UTC in this dataset. When simulations of r_o during canyon events are eliminated from the analysis, the comparison between WRF and the DIMM improves.
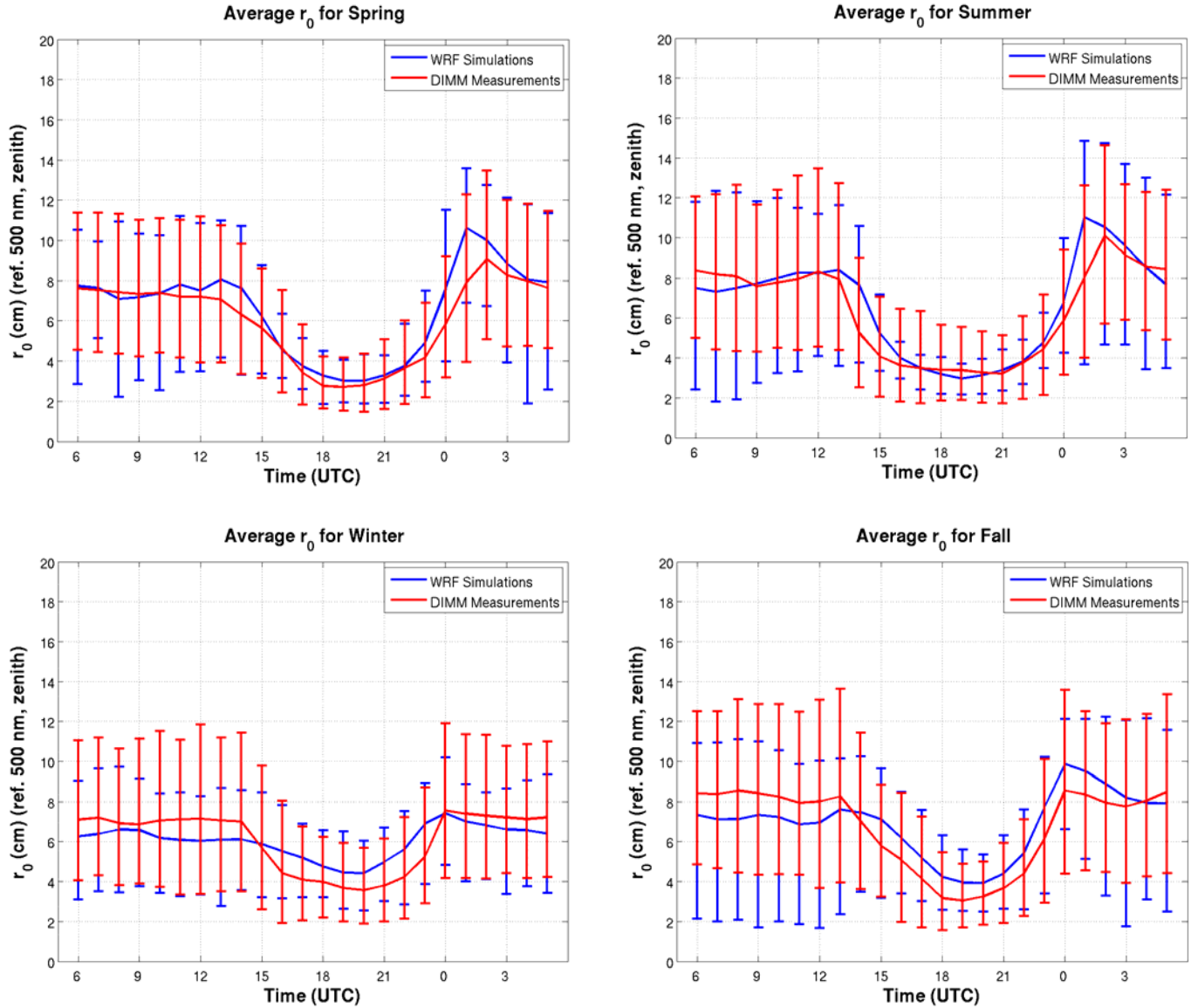
Figure 3. The diurnal variation in WRF simulated and PAODMS observed r_o **for (a) spring, (b) summer, (c) fall, and (d) winter**

Cumulative Distribution Functions (CDF) of r_o are shown for each season in Figure 4. For comparison purposes the CDF of the DIMM is overlaid. Only those simulations of r_o that had a cloud-free line of sight (CFLOS) are included in this analysis. This is done because the DIMM only makes measurements during CFLOS conditions. Regardless of the season, the comparison between WRF and the DIMM is quite good. As alluded to earlier, WRF does not simulate the smallest values of r_o due to the limited horizontal resolution for these particular runs. In addition, there are many more observations in the DIMM database than there are WRF points. This is mainly due to the limited number of clear simulations during each season. ABQ is cloudy up to 45% of the time. It is hypothesized that additional simulations over this region will increase the sample size and produce a more complete distribution of seeing parameters.
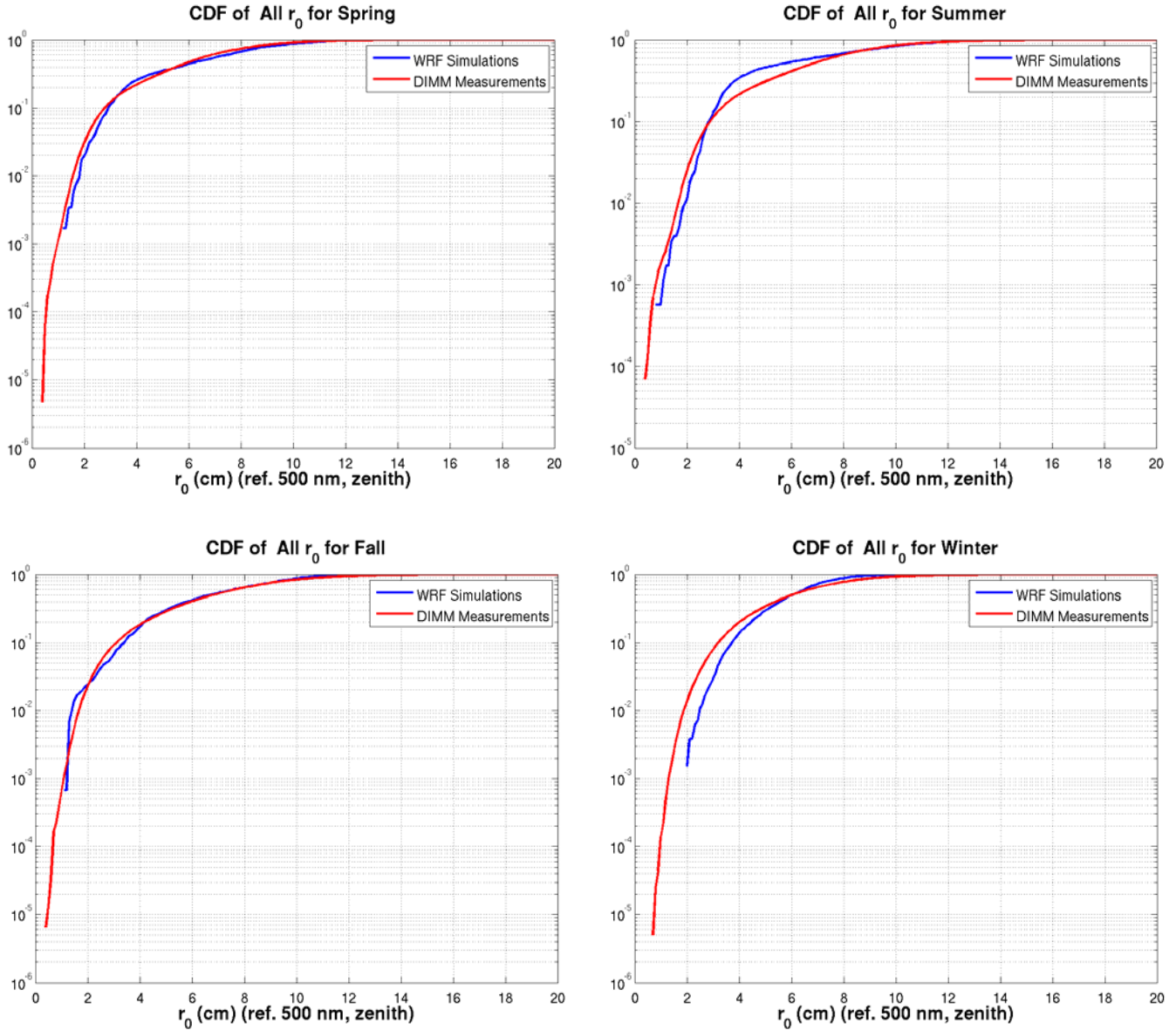
Figure 4. CDF of r_0 from WRF simulations and PAODMS observations for (a) spring, (b) summer, (c) fall, and (d) winter

Although the DIMM and other similar instruments are useful in collecting observations for a particular location, it is difficult to collect in many locations simultaneously. The infrastructure to maintain these instruments is large and expensive. However, HPC makes it very convenient and affordable to simulate turbulence over many areas simultaneously. With the help of the MHPCC Jaws system, it has been possible to produce many simulations from which the two-dimensional structure of r_0 can be characterized. Figure 5 shows a plot of two-dimensional r_0 over the New Mexico domain. Terrain and land usage are a large driver of turbulence in these simulations. Regardless of the time of day, the mountain tops of the Sandia and Manzano mountains have excellent seeing. In contrast, in the lower elevations values of r_0 are much smaller, particularly in areas near the Rio Grande river valley. As expected, however, overall r_0 values are larger during the early morning (1100 UTC) and smaller during mid-afternoon (2000 UTC). Although not shown, WRF also does an excellent job simulating the large difference in turbulence found between water and land. This is due to the reduced heat fluxes that are found over the water as compared to land. In addition, the diurnal variation of turbulence is also suppressed over the water compared to land due to the large heat capacity of water.
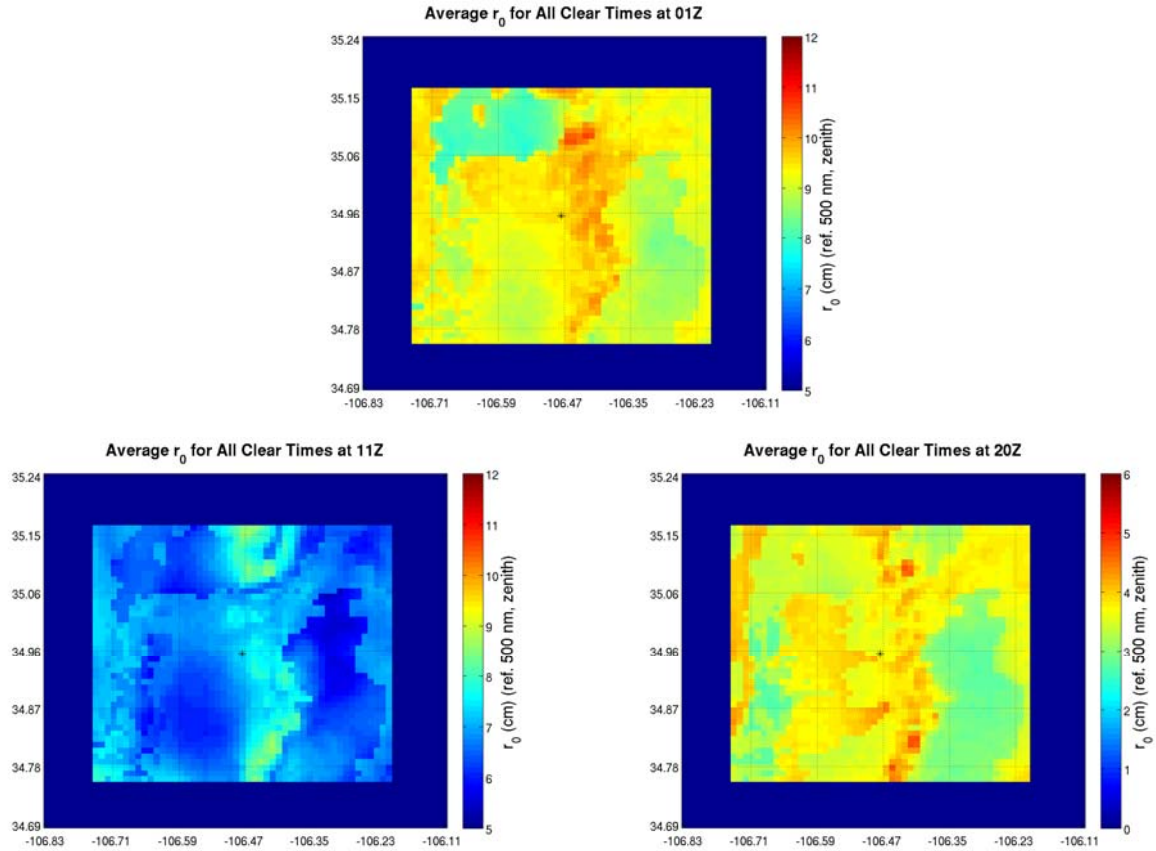
Figure 5. The two-dimensional distribution of r_o **as derived from the WRF model at (a) 0100 UTC, (b) 1100 UTC, and (c) 2000 UTC.** r_o **is shown in cm referenced to zenith.**

4. Summary and Conclusions

Simulations of OT were performed using the WRF model. Although the WRF model is incapable of simulating the very smallest values of r_o, it is capable of generally describing the climatology of the region of interest. This makes the model very convenient to use over areas where observations are not possible. The model does an excellent job simulating the diurnal variation found in turbulence. In addition, its ability to simulate regional variations as a function of the land type (e.g., water vs. land, mountain vs. valley, desert vs. forest) is quite profound. Comparisons to observations also showed a remarkable agreement.

5. Acknowledgments

References

Deardorff, J. W., 1980: Stratocumulus-capped mixed layers derived from a three-dimensional model. *Bound.-Layer Meteor.*, **18**, 495–527.

Fried, D. L., 1965: Statistics of a geometric representation of wavefront distortion. *J. Opt. Soc. Amer.*, **55**, 1427–1435.

Gerrity, J. P., T. L. Black, and R. E. Treadon, 1994: The numerical solution of the Mellor-Yamada level 2.5 turbulent kinetic energy equation in the Eta model. *Mon. Wea. Rev.*, **122**, 1640–1646.

Kondo, J., O. Kanechika, and N. Yasuda, 1978: Heat and momentum transfers under strong stability in the atmospheric surface layer. *J. Atmos. Sci.*, **35**, 1012–1021.

Mellor, G. L., and T. Yamada, 1982: Development of a turbulence closure model for geophysical fluid problems. *Rev. Geophys. Space Phys.*, **20**, 851–875.

Skamarock, W. C., J. B. Klemp, J. Dudhia, D. O. Gill, D. M. Barker, M. G. Duda, X.-Y. Huang, W. Wang, and J. G. Powers, 2008: A description of the advanced research WRF version 3. NCAR Technical Note, NCAR/TN-475+STR, 113 pp.

Tatarskii, V. I., 1971: The effects of the turbulent atmosphere on wave propagation. Technical Report, U.S. Department of Commerce, NTIS TT-68-50464, 472 pp.

Walters, D. L., and D. K. Miller, 1999: Evolution of an upper-tropospheric turbulence event—comparison of observations to numerical simulations. *Preprints, 13th Symposium on Boundary Layer Turbulence*, AMS, 157–160, Dallas, TX.